Discover Materials

Research

Transdermal microneedle patch for antioxidants release

Samuel Mugo[1] · **Scott Robertson**[1] · **Weihao Lu**[1]

Received: 29 June 2024 / Accepted: 12 March 2025
Published online: 22 March 2025

Abstract
Polymer based microneedle transdermal drug delivery system fits the criterion for an efficient patient compliant drug delivery system of the future. Smart and controlled microneedle drug delivery systems remain an emerging research area. One of the objectives of this study was to design an accessible approach of molding microneedles using a beeswax mold. The second objective was to evaluate a polymer-based microneedle drug release transdermal platform fabricated via layer by layer (LbL) assembly of conductive polydimethylsiloxane integrated with carbon nanotubes, cellulose nanocrystal and polyaniline (PDMS@CNT/CNC@PANI). The electrically conductive PDMS@CNT/CNC@PANI microneedle patch provides a platform for drug loading, stabilization and transdermal controlled drug release. The drug loaded PDMS@CNT/CNC@PANI microneedle patch was evaluated for diffusion and voltage mediated transdermal delivery of thymol blue and rutin as model compounds. Chicken skin was used as an analogue of human skin. Both electrochemical and passive release from the rutin loaded PDMS@CNC/CNT microneedle patch resulted in ~ 66%. On the other hand, the PDMS@CNC/CNT@PANI patch loaded with rutin resulted in 66–84% release. The results show the novel microneedle patches could effectively release rutin in a controlled manner, and as such showed promise for potential use in clinical drug release applications.

Graphical Abstract

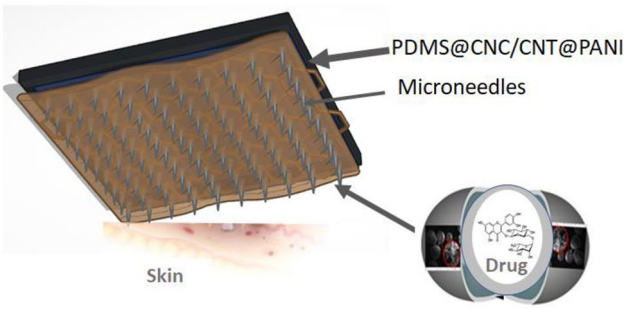

Keywords Transdermal drug delivery · Polymer microneedle patches · Electrochemotherapeutic platforms · Antioxidant controlled release

Supplementary Information The online version contains supplementary material available at https://doi.org/10.1007/s43939-025-00240-8.

✉ Samuel Mugo, mugos@macewan.ca | [1]Physical Sciences Department, Macewan University, 10700-104 Avenue, Edmonton, AB T5J 4S2, Canada.

1 Introduction

Appropriate drug delivery remains a key determinant of therapeutic health outcomes. Common drug delivery methods include oral ingestion and hypodermic needle injections. For some therapeutics, oral drug administration is low in efficacy and poses gastrointestinal side effects. Intravenous injection requires a trained health practitioner, causes tissue damage, and has poor patient compliance. Transdermal drug delivery is a desirable alternative that mitigates deficiencies of conventional drug delivery methods [1, 2]. A practical challenge for transdermal drug delivery is the skin's stratum corneum barrier layer, which severely limits the range of deliverable compounds, allowing only passive diffusion of small lipophilic molecules [3]. Microneedles have revolutionized the field of transdermal therapeutics delivery as they combine the ease of drug administration of traditional drug delivery while mitigating the deficiencies [3, 4]. Moreover, microneedle assisted transdermal delivery reduces the lag time of drug bioavailability in the bloodstream compared to unassisted transdermal delivery [5]. Microneedles are typically < 1 mm in length and painlessly penetrate the stratum corneum barrier by creating micro-punctures through the skin [1]. This action greatly enhances permeability efficiency, and enables the transdermal delivery of larger molecules, such as nucleic acids and peptide chains [6–9]. Additionally, microneedles can lend well for combination with other transdermal drug delivery enhancing strategies, such as iontophoresis or electroporation, which results in increased delivery efficacy [10].

Common microneedle delivery methods are made from silica, ceramics, stainless steel, and titanium [11]. While these common microneedles often display respectable mechanical strength [12], they generally have a higher cost due to their complexity in fabrication. Carbohydrate microneedles remedy the high cost but lack versatility in the scope of drug binding [11]. Polymeric microneedles are desirable due to their ease of fabrication, physical durability, and their versatility for tailored drug binding. In polymer platforms, drugs are adsorbed on the microneedle array or incorporated within polymers during polymerization [1]. Due to their structural tailorability in their chemical synthesis, polymers are versatile and accommodate a diverse range of drug delivery and release mechanisms [13]. Polymers afford specific drug binding and controllable drug release properties such as with the stimuli-responsive polymers—designed to release drugs in response to chemical or physical triggers such as changes in pH, electrical field, magnetic field, temperature, etc. [13].

Optimization of the composition and mechanical characteristics of polymeric microneedles is critical to ensuring effective drug delivery. The ability for the microneedle to withstand insertion forces is necessary for optimal perforation of skin and is dependent on many physical factors such as needle sharpness, length, base diameter, spacing, materials toughness, and patch thickness [14, 15]. Solid materials such as carbon nanotubes (CNTs) or reduced graphene oxide (rGO) can be implanted within the polymer matrix as a filler, enhancing physical toughness [16, 17]. These materials also impart conductive properties to the polymer, which enables it to potentially be used for electroporation or iontophoretic purposes with inherent synergistic effect for drug delivery [16, 17].

Polymer microneedles remain an emerging technology desirable for transdermal electrochemo-therapeutics, with more improvement in design necessary for widespread application. In this article demonstrate a very simple approach to fabricate a microneedle mold from beeswax, which to our knowledge has not been reported elsewhere in literature. We demonstrate herewith a conductive microneedle transdermal platform fabricated by layer-by-layer assembly (LbL) of polydimethylsiloxane integrated with carbon nanotubes and cellulose nanocrystal (PDMS@CNC/CNT) and a similar variation with an additional polyaniline (PANI) layer (PDMS@CNC/CNT@PANI). We demonstrate these microneedle patches have potential application for non-invasive voltage-stimulated transdermal delivery. As a proof of concept, we evaluated thymol blue and rutin, an antioxidant, as model compounds. Thymol blue is a pH-sensitive compound that shares structural similarities and chemical properties with many drugs. Thymol blue is strong chromophore making it suitable for experimental spectrometric measurements of its mobility behavior in drug delivery systems [18]. Rutin, a bioflavonoid found in plants like apples, figs, and tea, possesses strong antioxidant properties [19]. Rutin's high molar absorptivity enables precise absorbance measurement of its mobility during simulated drug delivery. While porcine skin is probably the most used, it has been demonstrated the widely accessible chicken skin is an effective transdermal analogue and as such was used in this article [20, 21].

2 Materials and methods

2.1 Materials

The multi-walled carboxylic acid functionalized carbon nanotubes (CNTs) (OD: 4–6 nm. 98% pure) were purchased from TimesNano, China. Aniline (ANI), ammonium persulfate (APS), thymol blue, 3-(trimethoxysilyl)propyl methacrylate (TPM), sulfuric acid, potassium ferricyanide ($K_3[Fe(CN)_6]$), isopropyl alcohol, diethylamine, methanol, ethanol, cyclohexanol, and rutin (95%), were obtained from Sigma Aldrich, Oakville, Ontario Canada. The Dow and Corning's Sylgard 184 polydimethylsiloxane (PDMS) silicone base and curing agent was purchased from Dow Corning Corporation, Midland, Michigan, United States. The Ecoflex 00–30 part A and part B was bought from Smooth-on Incorporation, Edmonton, Alberta, Canada. Cellulose nanocrystals (CNC) was donated by Alberta Innovates, Canada. All aqueous solutions were prepared using > 18 MW Milli-Q deionized (DI) water.

2.2 Conductive PDMS@CNC/CNT microneedle patch fabrication

To fabricate the microneedle PDMS patch, 15 g of beeswax was melted in a glass container (10.0 × 15.0 × 6.5 cm) and allowed to solidify. Template female microneedles were printed on the beeswax mold by stamping with a microneedle roller (M.T. brand, model MT2.5, needle dimension 0.25 mm). A 20 g of PDMS prepolymer mixture containing 45% PDMS silicone base, 5% PDMS curing agent, 25% EcoFlex 00–30 Part A and 25% EcoFlex 00–30 Part B (w/w), was poured onto the female microneedle wax mold and cured at room temperature for one week. The male microneedle PDMS patch was then peeled off the beeswax mold, resulting in a microneedle array, each needle having a length of ~ 250 µm. The microneedle PDMS patches were cut into 1 × 1.5 cm segments, with 110 microneedles per patch. To impart conductivity on the microneedle PDMS patch, a thin layer of 0.15 g of conductive PDMS@CNC/CNT gel (composition delineated vide infra) was spread evenly using a glass rod, followed by overnight curing at 80 °C. The conductive PDMS@CNC/CNT gel printed on the microneedle PDMS patch was prepared by mixing 0.2 g multiwalled CNTs, 0.2 g CNC, 7 mL of toluene, 800 µL of 1000 ppm naphthalene dissolved in acetonitrile, 1.9 g Sylgard 184 PDMS base, and 0.2 g silicone curing agent. To ensure homogeneity of the suspension, CNT and CNC was first suspended in toluene and naphthalene and sonicated for 1 h. Subsequently, the 1.9 g Sylgard 184 PDMS silicone base was then added to the homogeneous CNT/CNT suspension and sonicated for 1 h. The suspension was stirred using a stir plate at 50 °C for 24 h to evaporate all toluene. Finally, 0.2 g of Sylgard 184 PDMS curing agent was added to the suspension and thoroughly mixed with a glass stirring rod, resulting in a highly viscous and homogeneous conductive gel.

2.2.1 Integration of the conductivity enhancing PANI layer to the PDMS@CNC/CNT substrate

To enhance conductivity of the microneedle PDMS@CNC/CNT patches, a PANI layer was added. A prepolymer mixture comprised of 0.2 M aniline, 1 mg/ml CNT, 4 mg/mL CNC, and 1 M H_2SO_4 was prepared. The mixture was created by first adding 12 mg CNC to 2.3 mL DI water and stirring overnight, followed by adding 3 mg CNT and sonicating the mixture for 6 h to create a homogenous suspension. Subsequently, 0.6 mL of 5 M H_2SO_4 and 54 µL of aniline was added to the homogeneous CNC/CNT suspension. A 10 µL PANI prepolymer mixture aliquot with 5 µL of 1.5 M APS initiator was evenly spread on the microneedle PDMS@CNC/CNT patch and left to polymerize on an ice block for 45 min. Following polymerization, the PDMS@CNC/CNT/PDMS@PANI was left overnight in a dehydrator at 40 °C to dry. Figure 1 shows the schematic of the step by step process of fabricating the PDMS@CNC/CNT@PANI microneedle patches.

2.2.2 Loading compounds onto microneedle patches

Thymol blue and rutin were evaluated as model drugs. A 100 µL aliquot of either thymol blue (1 mg/mL in 95% ethanol, or 5 mg/mL in 20:80 v/v diethylamine:isopropyl alcohol), or rutin (5 mg/mL in 20:80 v/v diethylamine:methanol) was drop-casted on the surface of each test microneedle patch, and air-dried prior to analysis.

2.3 Voltammetric and spectrophotometric evaluation of patch drug release

Cyclic voltammetry (CV) on the drug loaded microneedle patches was used as a mode for voltage stimulation and to monitor drug release. The CV was acquired using PSTrace software (PalmSens BV, Netherlands). Voltammograms were

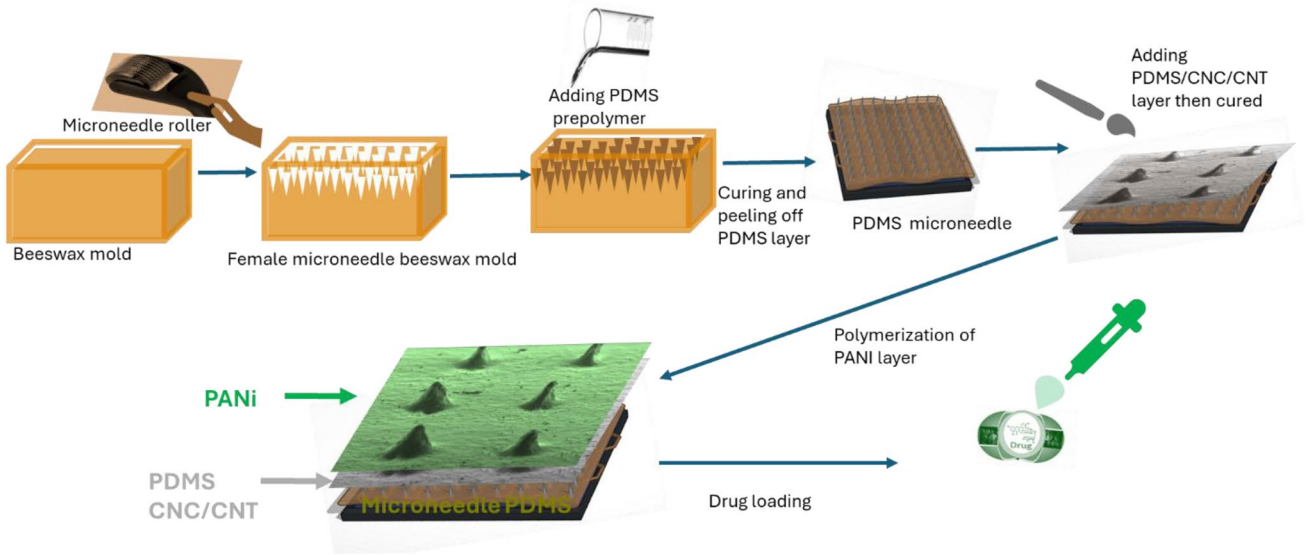

Fig. 1 Schematic showing the fabrication of the PDMS@CNC/CNT@PANI microneedle patches

obtained by immersing the drug loaded microneedle patches in 10 mL of 0.1 M phosphate buffer (pH = 7.1) in an electrochemical cell, with a platinum auxiliary electrode, and an in-house fabricated Ag/AgCl reference, fabricated as described elsewhere [22]. The microneedle patch drug release kinetics study was carried out by applying CV scans (−1.5 to + 1.5 V range, 0.1 V/s scan rate). During voltage stimulation by CV, the drug release into the buffer was simultaneously monitored by spectrophotometry, using SpectroVis Plus spectrophotometer with a LabQuest 2 device (Vernier). Absorbance readings were taken following duplicate CV scans. Passive release data was acquired by immersing the drug-loaded patch in PBS and measuring the absorbances in a trend mirroring that of the voltage-mediated release.

2.4 Voltammetric and spectrophotometric evaluation of antioxidant release into skin mimic

Skin mimics were produced by folding a square of tissue paper into an ~ 0.5 cm thick, 3.0 × 1.5 cm rectangle. The tissue paper was then soaked in a 10% PDMS (in the conventional 10:1 ratio for elastomer to curing agent) in cyclohexanol (w/w), followed by curing at 70 °C overnight. Cyclohexanol was used as a diluent for PDMS prepolymer. While solvents such as toluene could also be used their vapor pressure is too high and as such evaporates before curing. On the other hand, cyclohexanol has low vapor pressure and dissolves the PDMS prepolymer while following curing and effective stable firm is obtained.

Prior to voltammetric analysis, the paper-based skin mimics were soaked in 0.1 M (pH = 7.1) PBS for 30 min. The Ag/AgCl reference and platinum counter electrodes were pressed into the surface of the skin mimic, and the drug (thymol blue or rutin)-loaded microneedle patch was pressed into the skin mimic whilst simultaneously being held by the alligator clips of the voltammetric apparatus. For voltage mediated release, 20 CV cycles (−1.5 to + 1.5 V; 0.1 V/s; over 20 min) were applied to the microneedle patch. The CV runs were acquired in duplicate. The current signals from the voltammograms were averaged over the 0—0.8 V range, and the capacitance of the patch calculated by taking the ratio of current to scan rate (V/s). For passive diffusion (no voltage application), the microneedle patch was left standing on the buffer soaked skin mimic for 20 min. No spectrophotometric release trend was identified for either release method, instead, the total amount of rutin released into skin after 20 min was analyzed. To extract rutin, the skin mimic was soaked and vortexed with 3 mL methanol, and extraction repeated four times, and the extract analyzed by spectrophotometry.

2.5 Voltammetric and spectrophotometric evaluation of antioxidant release into chicken skin

Small cutlets from a chicken thigh were soaked in 0.1 M (pH = 7.1) PBS overnight prior to analysis. The Ag/AgCl reference and platinum counter electrodes were pressed into the PBS soaked cutlet, and the rutin-loaded microneedle patch pressed into the chicken skin whilst simultaneously being held by the alligator clips of the voltammetric apparatus. For voltage mediated release, 30 CV cycles (−1.5 to + 1.5 V; 0.1 V/s) were applied to the microneedle patches and rutin release

was monitored by CV as well as spectrophotometry. The CV scans were acquired in duplicate and the currents from the voltammograms averaged over the 0–0.8 V range. Capacitance was calculated by taking the ratio of current to scan rate (V/s). For passive release, the microneedle patch was similarly pressed onto the chicken cutlets whilst being held by alligator clips for a total of 30 min. No spectrophotometric release trend was identified, instead, the total amount of rutin released into skin after 30 min was analyzed. The chicken skin had rutin washed off the surface by copious amounts of D.I water, and the remaining rutin was extracted by vortexing the cutlet in 4 mL of methanol for one min, and the extraction repeated four times. The extract was then centrifuged (5000 rpm, 10 min) and analyzed via spectrophotometry.

2.6 Electrochemical impedance spectroscopy evaluation of the microneedle patches

Electrochemical impedance spectroscopy (EIS) was used to characterize the microneedle PDMS@CNC/CNT and PDMS@CNC/CNT@PANI patches. Nyquist plots were acquired by immersing the microneedle patches in 10 mL of 25 mM $K_3[Fe(CN)_6]$ in KCl as a standard redox probe in an electrochemical cell, with an in-house fabricated Ag/AgCl reference, and a platinum auxiliary electrode. The EIS was acquired in duplicate using Palmsens 4 potentiostat, and circuit fitting was done using PStrace software (PalmSens BV, Netherlands).

3 Results and discussion

3.1 Characterization of microneedle patches

The microneedle PDMS@CNC/CNT and PDMS@CNC/CNT@PANI patches were first characterized by FTIR to confirm the fabrication of each layer. Figure 2 shows the overlapped IR spectra. Both patches had characteristic peaks including 792 cm^{-1} attributed to Si–C stretching vibration, 864 cm^{-1} related to Si-CH_3 rocking, 1006 cm^{-1} related to Si–O-Si stretching vibrations [23] and the broad bands around 530 cm^{-1} assigned to Si–O-Si bending vibration [24]. These silicone-based peaks decreased in intensity with subsequent addition of the PANi layer (Fig. 2). The PDMS@CNT/CNC/PDMS@PANI had characteristic peaks at 1296–3121 cm^{-1} and 1413–1454 cm^{-1} assigned to the C-N stretching and C = C stretching vibrations of benzenoid and quinoid rings, indicative of PANI formation [25].

The morphology of the microneedle patches were characterized using SEM. Figure 3a shows the SEM image of the PDMS@CNC/CNT patches with well defined ~ 250 µm tall microneedle structures with distances of ~ 650 µm between microneedles. Each 1 × 1.5 cm patch had 110 microneedles. The microneedle patches were further characterized by EIS. Figure 3b shows the nyquist plots from analysis of 25 mM K_3FeCN_6 solution in 0.1 M PBS for PDMS@CNC/CNT and PDMS@CNC/CNT@PANI patches, respectively. It is known that the smaller the semicircle in the high frequency region of the nyquist plots, the smaller is the value of electron transfer resistance (R_{ct}). A low R_{ct} value is indicative of low electrode surface electron transfer resistance and thus greater electrode transducing capabilities. Using the Randles equivalency

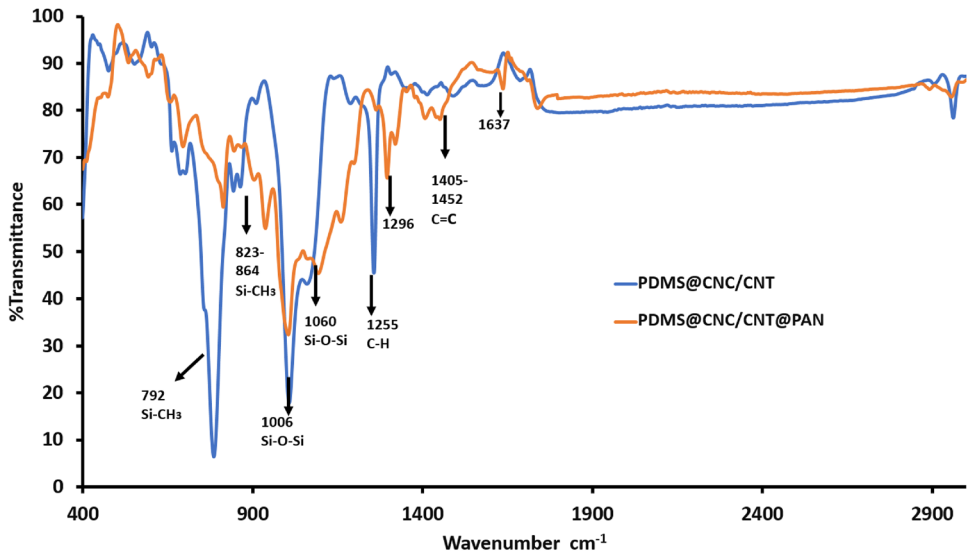

Fig. 2 Overlapped FTIR spectra for microneedle PDMS@CNC/CNT and PDMS@CNC/CNT@PANI patches

circuit for fitting the EIS plots (Fig. 3c), the R_{ct} values for the PDMS@CNC/CNT and PDMS@CNC/CNT@PANI patches were 3573 Ω, and 2309 Ω, respectively.

The conductivity of the microneedle PDMS@CNC/CNT patch evidences a good dispersion achieved between the PDMS insulating matrix and the CNC/CNT with the appropriate choice of the toluene and naphthalene solvent system, reported previously to preserve the excellent electrical property of CNTs [26]. There was a decrease in the observed R_{ct} value after integration of the PANI layer to the PDMS@CNC/CNT which was due to the increased electron transfer sites and a large surface area for the electrode patch. Evident in Fig. 3d, the enhanced conductivity can be attributed to the synergistic effect of the interpenetrating network bridging structures of PANI emeraldine salt domains to the CNT, thus inducing a charge transfer from PANI quinoid unit to CNT [22].

The electroactive surface area of the microneedle patches was further characterized by running CV of the redox couple 25 mM K_3FeCN_6 in 0.1 M PBS at different scan rates (0.02, 0.04, 0.06, 0.08, and 0.1 V/s) and invoking the Randles–Sevcik equation [23, 27]. Fig. S1 shows the resulting linear profiles for cathodic and anodic peak current as a function of the square root of scan rates for the different microneedle patches. Evidently, the electroactive response was highest for PDMS@CNC/CNT@PANI microneedle patch due to the increased synergy in conductivity between the CNT and the PANI, collaborated in the overlapped CVs in Fig. 3d. Using the Randles–Sevcik equation for the cathodic current [23], the surface areas for the PDMS@CNC/CNT and PDMS@CNC/CNT@PANI microneedle patches were calculated to be 0.0156 mm^2 and 2.69 mm^2, respectively.

3.2 Evaluation of microneedle patches for thymol blue release

The microneedle PDMS@CNC/CNT and PDMS@CNC/CNT@PANI patches were evaluated for drug loading and release kinetics, using thymol blue as a model compound. Fig. S2 shows the overlapped voltammograms obtained from PDMS@CNC/CNT and PDMS@CNC/CNT@PANI microneedle patches. Capacitance was used as a non-quantitative metric indicative of electrochemically stimulated drug release. Figure 4a shows the time release kinetics of thymol blue loaded PDMS@CNC/CNT and PDMS@CNC/CNT@PANI patches, using ethanol as the thymol blue loading solvent, under electrochemical stimulation. Ethanol is relatively non-penetrative to PDMS [28], and as such, the drug is largely expected to be adsorbed on the polymer matrix surface. In both patches, the capacitances increased linearly in the first 8 min, indicative of gradual controlled release of the electrically insulating thymol blue compound from the patch surface (Fig. 4a). Notably, due to its inherent high conductivity, the PDMS@CNC/CNT@PANI patch resulted in more rapid thymol blue release under

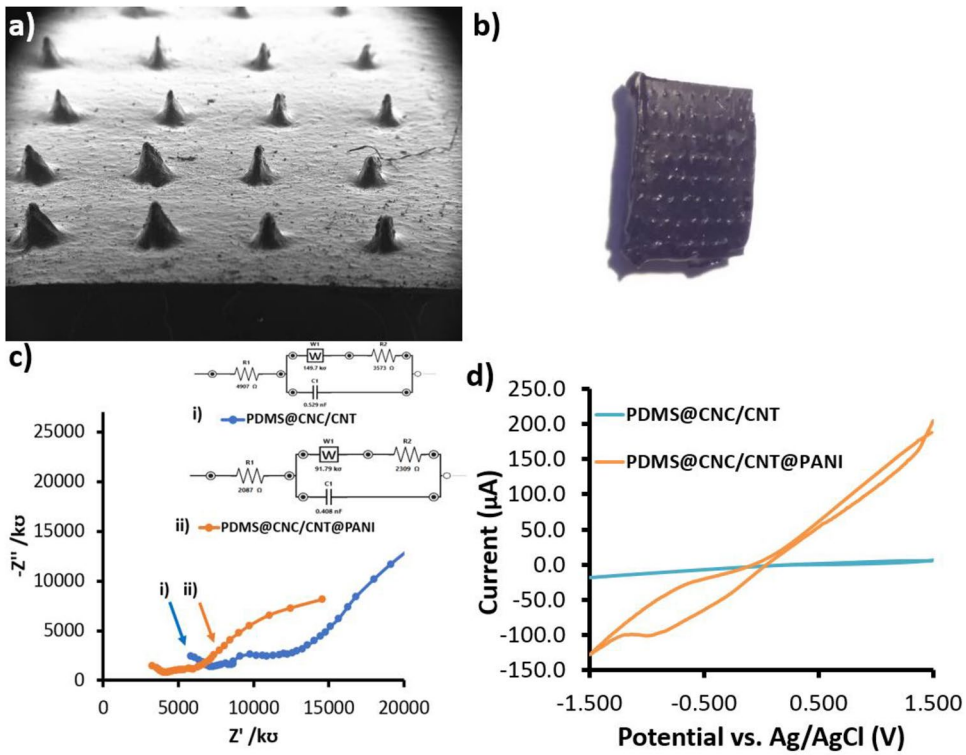

Fig. 3 **a** SEM of microneedle PDMS@CNC/CNT patch; **b** Camera image of microneedle PDMS@CNC/CNT; **c** EIS Nyquist plot and Randles Circuit for i) PDMS@CNC/CNT and ii) PDMS@CNC/CNT@PANI microneedle patches; and **d** Cyclic voltammogram (0.02 V/s scan rate) of microneedle PDMS@CNC/CNT and PDMS@CNC/CNT@PANI patches in 25 mM K_3FeCN_6 solution in 0.1 M PBS

electrochemical stimulation compared to the PDMS@CNC/CNT, evident by the nearly doubled slope in the capacitance kinetics profile (Fig. 4a). For the PDMS@CNC/CNT patch, the capacitance profile plateaus after ~ 8 min, while the PDMS@CNC/CNT@PANI peaks at ~ 6 min, and then decreases, both trends are indicative of complete drug release from the patch (Fig. 4a).

Voltage-mediated release of thymol blue loaded onto PDMS@CNC/CNT and PDMS@CNC/CNT@PANI patches using PDMS-penetrating diethylamine:isopropyl alcohol (20:80 v/v) solvent system [28] was also examined (Fig. 4b). The PDMS penetrative solvent system enhances drug integration in the polymer matrix increasing loading and stability [24]. In both patches, the capacitances increased linearly in the first 10 min, before plateauing, indicating most of the thymol blue was released from the patches (Fig. 4b). Over the 10 min linear range, the PDMS@CNC/CNT@PANI showed a 6.7 times steeper slope in the kinetics profile compared to PDMS@CNC/CNT, indicative of the faster drug release due to the higher conductivity imparted by the PANI layer (Fig. 4b).

Quantitative evaluation of the drug loading and release was determined using spectrophotometry (Fig. 4c and d). Using ethanol as a non-PDMS penetrating solvent [24], the amount of thymol blue loaded on both PDMS@CNC/CNT and PDMS@CNC/CNT@PANI patches was determined to be ~ 0.1 mg/patch. Conversely, 0.5 mg of thymol blue was loaded on each patch using the PDMS-penetrating diethylamine/isopropyl alcohol solvent system (20:80 v/v) [28]. The patches with high drug loading were evaluated under passive and voltage stimulation conditions by immersing them in a 10 mL of 0.1 M PBS buffer (pH = 7.1) and the amount of thymol blue released in the buffer was determined by spectrophotometry. Fig. S2c. shows a representative overlapped spectra of thymol blue released in the buffer.

Electrochemically stimulated thymol blue release was also compared to passive mode (no voltage application). Results show that thymol blue loaded patch release kinetics were independent of electrochemical stimulation, regardless of loading solvent used (Fig. 4c and d). Using the ethanol loading solvent, both voltage-mediated and passive release of thymol blue from PDMS@CNC/CNT and PDMS@CNC/CNT@PANI patches begin to plateau at 4 –5 min. (Fig. 4c). The PDMS@

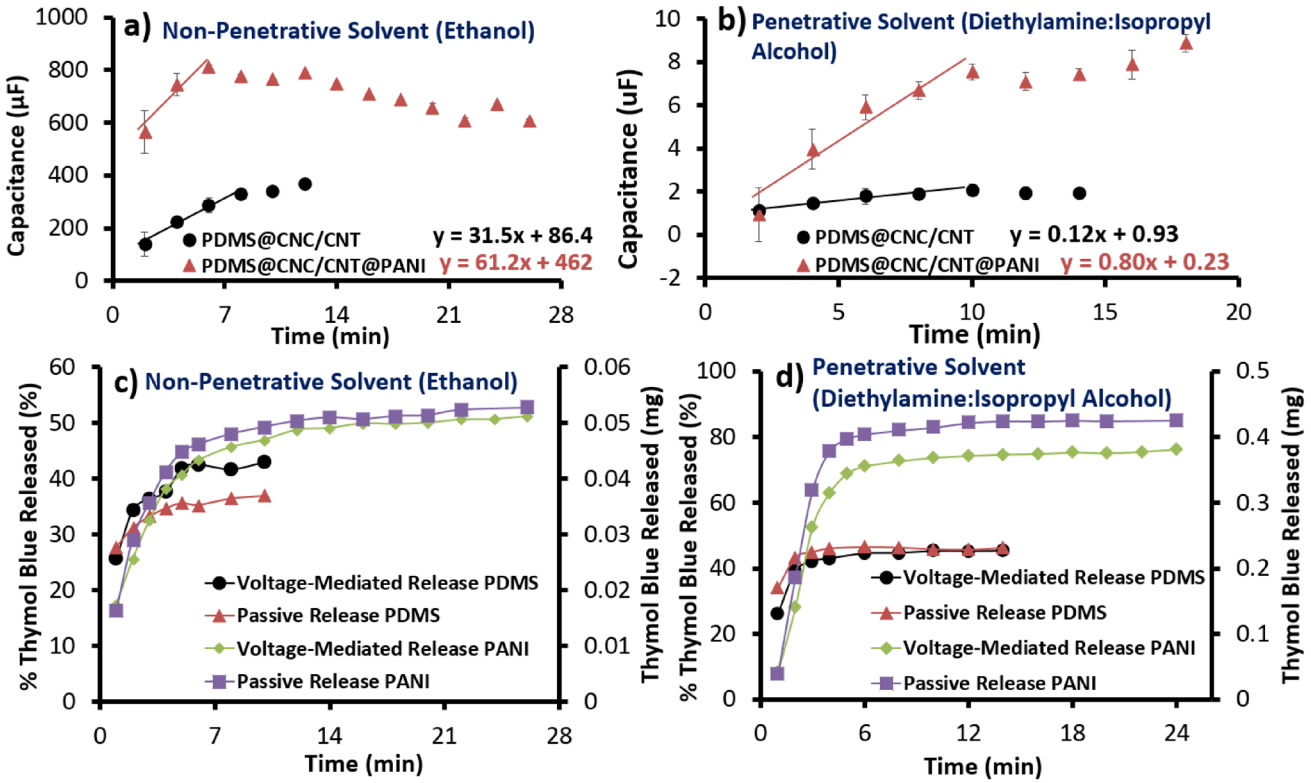

Fig. 4 **a** Voltammetric capacitance thymol blue patch release profile as a function of time using non-PDMS penetrating drug loading solvent; **b** Voltammetric capacitance thymol blue patch release profile as a function of time using PDMS penetrating drug loading solvent; **c** Spectrophotometric thymol blue patch release profile as a function of time using non-PDMS penetrating drug loading solvent system for PDMS@CNC/CNT (annotated in figure legend as PDMS)and PDMS@CNC/CNT@PANI (annotated in figure legend as PANI); **d** Spectrophotometric thymol blue patch release profile as a function of time using PDMS penetrating solvent, diethylamine/isopropanol for PDMS@CNC/CNT (annotated in figure legend as PDMS) and PDMS@CNC/CNT@PANI (annotated in figure legend as PANI). The analytical wavelength was 437 nm for both **c**) and **d**)

CNC/CNT patch released 43% and 37% via voltage-mediated and passive release, over a period of 12 min, respectively (Fig. 4c). On the other hand, PDMS@CNC/CNT@PANI patch released approximately 53% and 51% of the drug cargo via voltage-mediated and passive release, over a period of 26 min, respectively (Fig. 4c).

Drug loading and release was however significantly affected by the solvent used to load the drug. As shown in Fig. 4d, for both passive and electrochemically mediated release, the diethylamine/ isopropyl alcohol (20:80 v/v) thymol blue loaded patches release begins to plateau at 2 min for the PDMS@CNC/CNT patches, and 5 min for PDMS@CNC/CNT@PANI. However, the latter has a higher thymol blue cumulative drug release of ~ 76% and 85% via voltage-mediated and passive release, over a period of 24 min, respectively. This is compared to the PDMS@CNC/CNT base release of ~ 45% and 46% (in 14 min) for both voltage mediated and passive release, respectively (Fig. 4d). Both our patch designs demonstrate the ability to stably adsorb and release the model compound, thymol blue, into PBS buffer. While release efficacy was not enhanced by voltage application, all patch designs were shown to rapidly release thymol blue. The voltage mediated release would be drug dependent However, it is evident the PDMS@CNC/CNT@PANI patch has increased efficacy for cumulative drug release which can be explained by its inherent higher surface area, as evidenced by Randles–Sevcik results compared to PDMS@CNC/CNT. The additional layer of PANI while affording the increased surface area for drug release, contributes to the delayed release as the drug diffuses out of the multiple layers.

3.3 Evaluation of microneedle patches for rutin antioxidant release

The PDMS@CNC/CNT and PDMS@CNC/CNT@PANI microneedle patches were evaluated for loading and release of anti-aging agents such as rutin. Flavonoids such as rutin and other antioxidants such as resveratrol, baicalin, and vitamin E have been shown to improve the condition of wrinkles and skin elasticity in humans [29, 30]. Antioxidants are known to be effective scavengers of reactive oxygen species (ROS) such as ($O_2^{\bullet-}$, $OH^{\bullet}$, H_2O_2), which otherwise induce cellular damage and compositional loss of the skin extracellular matrix, resulting in sagging, wrinkles, loss of firmness and elasticity, and dryness [31–33].

Rutin was loaded onto the PDMS@CNC/CNT and PDMS@CNC/CNT@PANI microneedle patches using diethylamine/methanol (20:80 v/v) solvent system, determined to afford a higher loading and encapsulation stability due to its PDMS penetration [28]. Stabilization of antioxidants in polymer matrices increases their radical-scavenging capabilities over a longer period [34]. As shown in Fig. 5, both CV and spectrophotometric data indicate release kinetics of rutin from the patches. Evident in Fig. 5a, the release of rutin from the patch under voltage-stimulation corresponds with increased capacitance and plateaus after the entire rutin release. Both PDMS@CNC/CNT and PDMS@CNC/CNT@PANI patches share a similar increasing linear capacitive release trend over 8 min, before the values level off (Fig. 5a).

Figure 4b shows the rutin release trend monitored by spectrophotometry for PDMS@CNC/CNT and PDMS@CNC/CNT@PANI patches. The rutin release behaviour of both patches are practically identical, with a rapid initial rutin release up to 2 min followed by a plateau (Fig. 5b). The PDMS@CNC/CNT patch released approximately 72% and 65% over the 12 min for voltage-mediated and passive release, respectively for the 0.505 mg of rutin loaded. On the other hand, the PDMS@CNC/CNT@PANI patches released approximately 75% and 82% via voltage mediated and passive

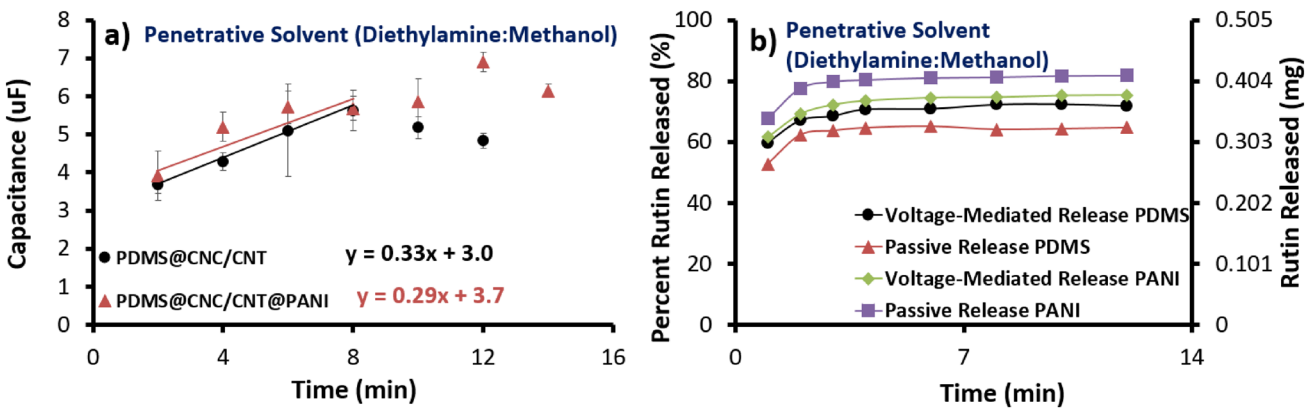

Fig. 5 **a** Voltammetric capacitance of rutin PDMS@CNC/CNT and PDMS@CNC/CNT@PANI patches release profile as a function of time; **b** Corresponding spectrophotometric rutin patch release profiles as a function of time using PDMS penetrating solvent diethylamine/methanol, determined at 392 nm

release over the 12 min, respectively (Fig. 5b). Similar to the thymol blue release trend examined previously, the electrochemical mediated rutin release did not present enhanced release performance (Fig. 5b). Regardless of this, each patch design offers rapid rutin release, desirable for daily therapeutics such as anti aging agents, or antioxidants.

3.4 Rutin release into hydrophobic tissue paper skin mimic

As a proof of concept for transdermal drug delivery, we evaluated the rutin loaded microneedle patch release into simulated skin prepared from a PDMS coated tissue paper as described in the methods section. The PDMS coated, buffer-soaked tissue paper was aimed to roughly mimic the hydrophobic nature of the human stratum corneum. The microneedle patches were loaded with rutin dissolved in diethylamine/methanol solvent system, to afford higher drug penetration to the polymer matrix, thus increasing loading and stability. The rutin release into the skin mimic was carried out using the experimental setup shown in Fig. 6a. The electrochemical data shows that rutin is released gradually over a period of 14 min, as evidenced by the linear increasing trend over this range, followed by a plateau. This trend was observed for both PDMS@CNC/CNT and PDMS@CNC/CNT@PANI patches (Fig. 6b). Evident from the slope values over the linear range from 0 to 14 min, the PDMS@CNC/CNT@PANI patch release the loaded rutin approximately 1.5 times faster than the PDMS@CNC/CNT patches (Fig. 6b). However, the PDMS@CNC/CNT microneedle patches, released between 73–95% of the 0.505 mg of loaded rutin via electrochemical-mediated and passive release (Fig. 6c). Comparatively, about 46–58% rutin was released for both passive and electrochemically induced PDMS@CNC/CNT@PANI patches (Fig. 6c). Determined by spectrophotometry, as shown it is evident that rutin was more completely released from PDMS@CNC/CNT compared to PDMS@CNC/CNT@PANI patches (Fig. 6c), which could be explained by the polarity effects of PANI that preferentially binds the rutin, hindering its complete release. The results demonstrate the PDMS@CNC/CNT compared to PDMS@CNC/CNT@PANI patches are effective for rapid delivery of rutin into the skin mimic, thus showing potential for transdermal drug release.

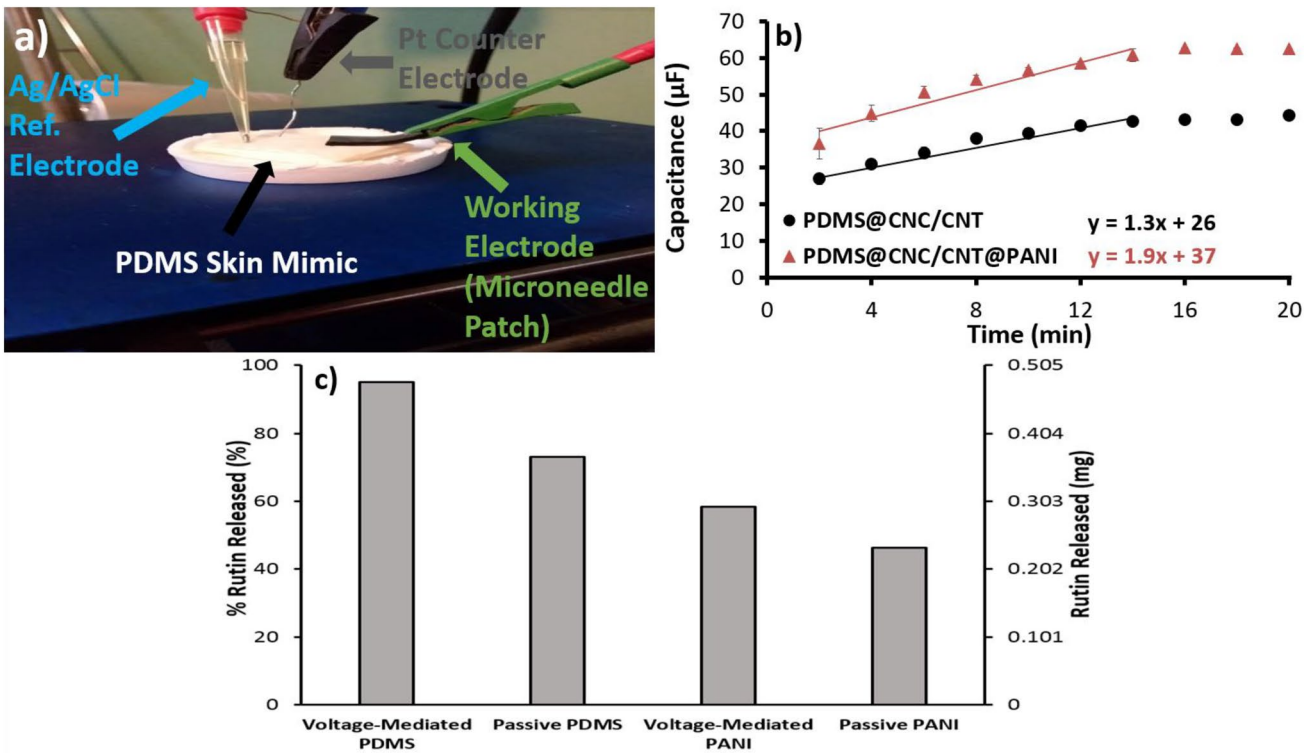

Fig. 6 **a** Voltammetric setup for hydrophobic tissue paper skin mimic antioxidant release test. **b** PDMS@CNC/CNT and PDMS@CNC/CNT@PANI microneedle patches rutin release into hydrophobic-tissue skin mimic using voltametric stimulation; **c** Comparative evaluation of the rutin release into skin mimic for PDMS@CNC/CNT and PDMS@CNC/CNT@PANI microneedle patches determined by spectrophotometry

3.5 Antioxidant release into chicken skin

To further prove the concept of the use of microneedle patches for transdermal release, rutin loaded PDMS@CNC/CNT and PDMS@CNC/CNT@PANI microneedle patches were evaluated for rutin delivery into the chicken skin, as an analog to human skin. The PDMS@CNC/CNT@PANI microneedles, which are shown to be ~ 250 µm in length (Fig. 2a), were found to be effective in perforating the chicken skin (Fig. 7a), which would prove the patch can allow the ease of drug diffusion across the ~ 20 µm thick stratum corneum layer of skin [35].

Similar to the previous experiments, the rutin was loaded on microneedle arrays using a diethylamine/methanol (20:80 v/v) solvent system. As shown in Fig. 7b with the voltage-mediated release of rutin into the chicken skin, the electrochemical response of microneedle PDMS@CNC/CNT compares closely to that of PDMS@CNC/CNT@PANI, indicating the rate of rutin release is very similar. Complete rutin release is observed in both patches to be ~ 12 min. Figure 7c shows the patches quantitative rutin release into the chicken skin through electrochemical mediated and passive diffusion as determined by spectrophotometry. Prior to spectrophotometric analysis, residual rutin was washed off the surface of the skin prior to extraction to demonstrate drug delivery into chicken skin was occurring. This was done to ensure that only the rutin that diffused past the stratum corneum layer was quantified. Both electrochemical mediated and passive release for PDMS@CNC/CNT microneedle patch were very similar, with ~ 66% of the 0.505 mg of loaded rutin released. The PDMS@CNC/CNT@PANI released between 66—84% of the 0.505 mg rutin loaded, under electrochemical stimulation and passive release conditions (Fig. 7c). The results demonstrate the microneedle patches are effective for release rutin in the hundred microgram range, with ease of scalability through change in rutin patch coverage for desirably higher dosages.

There is a clear distinction between passive and electrochemically mediated drug release, with the latter exhibiting higher release levels. However, electrochemical release is influenced by the redox properties of the drug, leading to variations in release patterns. Further research is needed to explore a broader range of drugs and their electrochemical release behaviors. While our findings show only modest differences between passive and electrochemically mediated

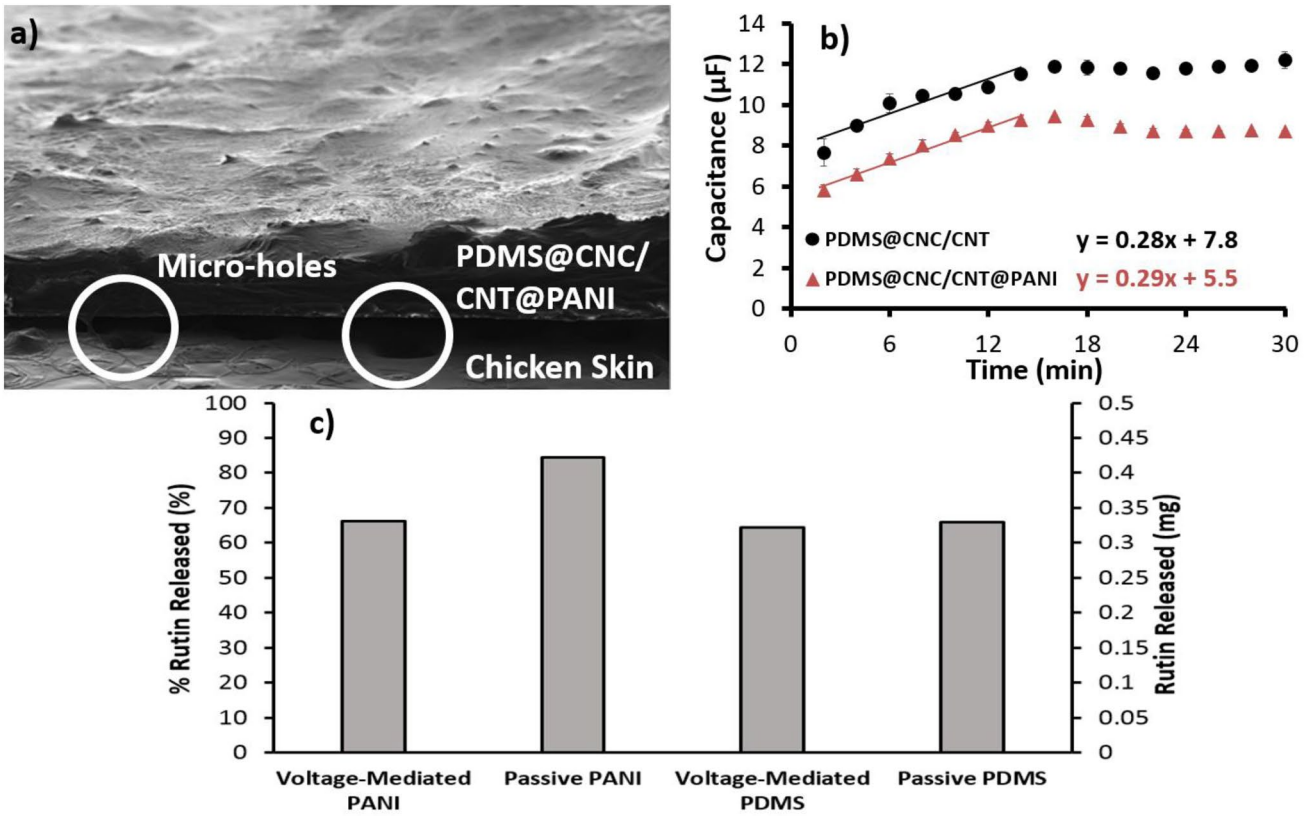

Fig. 7 **a** SEM of PDMS@CNC/CNT@PANI microneedle array and chicken skin cross-section; **b** PDMS@CNC/CNT and PDMS@CNC/CNT@PANI microneedle patches rutin release into into chicken skin; **c** Comparative evaluation of the rutin release into chicken skin for PDMS@CNC/CNT and PDMS@CNC/CNT@PANI microneedle patches determined by spectrophotometry

release, our approach offers significant advantages over conventional microneedles by enabling on-demand, localized drug delivery with minimal disruption to the skin barrier. Unlike iontophoresis or electroporation [10], which require charged drugs or higher energy inputs, our method allows for controlled release with minimal skin irritation and greater adaptability to different drug types.

It should be noted that chicken skin as a transdermal analogue has structural differences from human skin, including its thinner epidermis, reduced keratinization, differences in lipid composition, absence of sweat glands, and higher hydration levels, and as such can lead to overestimated drug permeability. Nonetheless, while porcine is the most widely used model, chicken skin can still provide valuable preliminary insights into transdermal drug delivery [20, 21].

While toxicity of nanoparticles is an issue of ongoing debate, CNTs are generally benign if rigidly immobilized within biocompatible polymers such as siloxane [36, 37]. As such, the highly stable PDMS@CNC/CNT@PANI microneedle patch is expected to be fully benign platform for transdermal applications.

4 Conclusion

Overall, we demonstrate the ability of our PDMS@CNC/CNT and PANI/CNC/CNT@PDMS microneedle patches for chemical loading and release, with thymol blue and rutin, used as model compounds. Both PDMS@CNC/CNT and PANI/CNC/CNT@PDMS patches had a similar release trend, with most of the loaded compounds released in under 5 min. The PDMS@CNC/CNT@PANI microneedle patches were found to be effective for penetration of the chicken skin, indicative for potential application in transdermal drug delivery in human use. In the future, the effectiveness of the microneedle patches for loading and voltage mediated release of other drugs with different hydrophobic and redox properties will be evaluated. In addition, future studies will involve standardized mechanical tests to quantitatively assess the microneedles' structural robustness, as well as evaluate clinical strategies for microneedle drug release via electric voltage application.

Acknowledgements Mugo research group acknowledges funding from Natural Sciences and Engineering Research Council of Canada (NSERC). Lisa Mugo from Archbishop MacDonald School is acknowledged for designing the microneedle sensor schematics.

Author contributions Credit Author Statement: Samuel M Mugo: Inception of the project design and its development to completion, supervision, funding acquisition, including revision of the manuscript. Scott Robertson: Methodology and experimentation, data validation and writing the original manuscript, and revising the manuscript. Weihao Lu: Methodology and experimentation, and data acquisition.

Funding The research was funded by Natural Sciences and Engineering Research Council of Canada (NSERC).

Data availability All data is available on request.

Declarations

Ethics approval and consent to participate The MacEwan Research Ethics Board and was consulted and cleared the use of chicken tissue in this experiment.

Consent for publication Not applicable.

Competing interests The authors declare no competing interests.

References

1. Wang M, Hu L, Xu C. Recent advances in the design of polymeric microneedles for transdermal drug delivery and biosensing. Lab Chip. 2017;17:1373–87.
2. Yang G, Zhang Y, Gu Z. Punching and electroporation for enhanced transdermal drug delivery. Theranostics. 2018;8:3688–90.

3. Nguyen HX, Bozorg BD, Kim Y, Wieber A, Birk G, Lubda D, Banga AK. Poly (Vinyl Alcohol) microneedles: fabrication, characterization, and application for transdermal drug delivery of doxorubicin. Eur J Pharm Biopharm. 2018;129:88–103.
4. Xiang Z, Wang H, Pant A, Pastorin G, Lee C. Development of vertical SU-8 microneedles for transdermal drug delivery by double drawing lithography technology. Biomicrofluidics. 2013;7: 066501.
5. Kochhar JS, Lim WXS, Zou S, Foo WY, Pan J, Kang L. Microneedle integrated transdermal patch for fast onset and sustained delivery of lidocaine. Mol Pharm. 2013;10:4272–80.
6. Henry S, McAllister DV, Allen MG, Prausnitz MR. Microfabricated microneedles: a novel approach to transdermal drug delivery. J Pharm Sci. 1998;87:922–5.
7. Huang D, Zhao D, Wang X, Li C, Yang T, Du L, Wei Z, Cheng Q, Cao H, Liang Z, Huang Y, Li Z. Efficient delivery of nucleic acid molecules into skin by combined use of microneedle roller and flexible interdigitated electroporation array. Theranostics. 2018;8:2361–76.
8. Ling MH, Chen MC. Dissolving polymer microneedle patches for rapid and efficient transdermal delivery of insulin to diabetic rats. Acta Biomater. 2013;9:8952–61.
9. Liu S, Zhang S, Duan Y, Niu Y, Gu H, Zhao Z, Zhang S, Yang Y, Wang X, Gao Y, Yang P. Transcutaneous immunization of recombinant staphylococcal enterotoxin b protein using a dissolving microneedle provides potent protection against lethal enterotoxin challenge. Vaccine. 2019;37:3810–9.
10. Kolli CS, Xiao J, Parsons DL, Babu RJ. Microneedle assisted iontophoretic transdermal delivery of prochlorperazine edisylate. Drug Dev Ind Pharm. 2012;38:571–6.
11. Larrañeta E, Lutton REM, Woolfson AD, Donnelly RF. Microneedle arrays as transdermal and intradermal drug delivery systems: materials science, manufacture and commercial development. Mater Sci Eng R Reports. 2016;104:1–32.
12. Cahill EM, Ocearbhaill ED. Toward biofunctional microneedles for stimulus responsive drug delivery. Bioconjug Chem. 2015;26:1289–96.
13. Wells CM, Harris M, Choi L, Murali VP, Guerra FD, Jennings JA. Stimuli-responsive drug release from smart polymers. J Funct Biomater. 2019;10:34.
14. Park JH, Allen MG, Prausnitz MR. Biodegradable polymer microneedles: fabrication, mechanics and transdermal drug delivery. J Control Release. 2005;104:51–66.
15. Kochhar JS, Quek TC, Soon WJ, Choi J, Zou S, Kang L. Effect of microneedle geometry and supporting substrate on microneedle array penetration into skin. J Pharm Sci. 2013;102:4100–8.
16. Skaria E, Patel BA, Flint MS, Ng KW. Poly(Lactic Acid)/carbon nanotube composite microneedle arrays for dermal biosensing. Anal Chem. 2019;91:4436–43.
17. Justin R, Chen B. Strong and conductive chitosan-reduced graphene oxide nanocomposites for transdermal drug delivery. J Mater Chem B. 2014;2:3759–70.
18. Eltaboni F, Al Balazi A, Al Warfaly MS. Thymol blue release from dried polyacrylamide filmogenic solution coated on a quartz cell one-shot study. J Chem Lett. 2024;5:128–33.
19. Guzman-Hernandez DS, Palomar-Pardave M, Sanchez-Perez F, Juarez-Gomez J, Corona-Avendano S, Romero-Romo M, Ramirez-Silva MT, Spectrochim M. Acta A Molecul. Biomol. Spectrosc. 2020;228: 117814.
20. Liu L, Li N, Chen M, Yang H, Tang Q, Gong C. Visible-light-responsive surface molecularly imprinted polymer for acyclovir through chicken skin tissue. ACS Appl Bio Mater. 2018;1:845–52.
21. Dawud H, Abu Ammar A. Rapidly dissolving microneedles for the delivery of steroid-loaded nanoparticles intended for the treatment of inflammatory skin diseases. Pharmaceutics. 2023;15:526.
22. Dhanjai SM, Mugo WLu. Modified stainless steel microneedle electrode for polyphenolics detection. Anal Bioanal Chem. 2020;412:7063–72.
23. Groza A, Surmeian A. Characterization of the oxides present in a polydimethylsiloxane layer obtained by polymerisation of its liquid precursor in corona discharge. J Nanomater. 2015. https://doi.org/10.1155/2015/204296.
24. Hospodarova V, Singovszka E, Stevulova N. Characterization of cellulosic fibers by FTIR spectroscopy for their further implementation to building materials. Am J Anal Chem. 2018;9:303–10.
25. Trchová M, Stejskal J. Polyaniline: the infrared spectroscopy of conducting polymer nanotubes (IUPAC technical report). Pure Appl Chem. 2011;83:1803–17.
26. Mulembo T, Nagai G, Tamagawa H, Nitta T, Sasaki M. Conductive and flexible multi-walled carbon nanotube/polydimethylsiloxane composites made with naphthalene/toluene mixture. J Appl Polym Sci. 2019;136:48167.
27. Habibi B, Jahanbakhshi M. A novel nonenzymatic hydrogen peroxide sensor based on the synthesized mesoporous carbon and silver nanoparticles nanohybrid. Sens Actuators B Chem. 2014;203:919–25.
28. Lee JN, Park C, Whitesides GM. Solvent compatibility of poly(dimethylsiloxane)-based microfluidic devices. Anal Chem. 2003;75:6544–54.
29. Farris P, Yatskayer M, Chen N, Krol Y, Oresajo C. Evaluation of efficacy and tolerance of a nighttime topical antioxidant containing resveratrol, baicalin, and vitamin E for treatment of mild to moderately photodamaged skin. J Drugs Dermatol. 2014;13:1467–72.
30. Choi SJ, Lee SN, Kim K, Joo DH, Shin S, Lee J, Lee HK, Kim J, Bin Kwon S, Kim MJ, Ahn KJ, An IS, An S, Cha HJ. Biological effects of rutin on skin aging. Int J Mol Med. 2016;38:357–63.
31. Rinnerthaler M, Bischof J, Streubel MK, Trost A, Richter K. Oxidative stress in aging human skin. Biomolecules. 2015;5:545–89.
32. Phaniendra A, Jestadi DB, Periyasamy L. Free radicals: properties, sources, targets, and their implication in various diseases. Indian J Clin Biochem. 2015;30:11–26.
33. Ahsanuddin S, Lam M, Baron ED. Skin aging and oxidative stress. AIMS Mol Sci. 2016;3:187–95.
34. Fonseca DFS, Vilela C, Pinto RJB, Bastos V, Oliveira H, Catarino J, Faísca P, Rosado C, Silvestre AJD, Freire CSR. Bacterial nanocellulose-hyaluronic acid microneedle patches for skin applications in vitro and in vivo evaluation. Mater Sci Eng C. 2021;118:111350.
35. Ye R, Yang J, Li Y, Zheng Y, Yang J, Li Y, Liu B, Jiang L. Fabrication of tip-hollow and tip-dissolvable microneedle arrays for transdermal drug delivery. ACS Biomater Sci Eng. 2020;6:2487–94.
36. Kim M, Goerzen D, Jena PV, Zeng E, Pasquali M, Meidl RA, Heller DA. Human and environmental safety of carbon nanotubes across their life cycle. Nat Rev Mat. 2024;9:63–81.
37. Dalla Colletta A, Pelin M, Sosa S, Fusco L, Prato M, Tubaro A. CARBON-BASED nanomaterials and SKIN: an overview. Carbon. 2022;196:683–98.